

Regular Articles

3D sound source localization with fiber optic sensor array based on genetic algorithm

Sekip Esat Hayber*, Serkan Keser

Department of Electrical-Electronic Engineering, Kırşehir Ahi Evran University, Kırşehir 40100, Turkey

ARTICLE INFO

Keywords:

Fiber optic sensor
 Fabry-Perot interferometry
 3D sound source localization
 Genetic algorithm
 Sensor array

ABSTRACT

Sound source localization (SSL), which is an area of multi-point acoustic detection, has always been an important research topic since it has been employed in many applications. It has been notable to use fiber optic sensors in the SSL due to the advantages compared to traditional sensors. In this paper, a fiber optic sensor array is obtained with sensor tips formed with polymer-based diaphragm material, which is low cost and easy to manufacture. The SSL process has been experimentally verified in the measurement medium with a volume of 1 m^3 . Both constant frequency sound signals and speech signals were used in experimental measurements. The signals received from the sensors were processed by using the genetic algorithm, and the average distance to the source was calculated in 3D with an error of 0.0248 m. In the measurements, results were obtained at very close distances to the sound source, such as 0.0032 m, 0.0046 m, 0.0071 m.

1. Introduction

Acoustics is a popular science that deals with the study of sound waves from infrasound to ultrasound [1]. Applications in acoustic science can be listed as the detection and location of cracks, internal stresses, evaluation of micro-displacements, earthquake prediction analysis through the detection of pressure, velocity monitoring, depth, sounding, submarine profiling, and non-destructive inspection of structures [2]. Furthermore, acoustic sensing is used in medical sciences, such as medical imaging, diagnosis, and detection of phase transitions. An acoustic transducer is at the basis of the system to be used in these applications [3]. Acoustic waves are mechanical pressure waves therefore, microphones have the same principle as a pressure sensor [4].

Some of the interesting features of fiber optic sensors (FOS) include their real-time display, fast response, stability, wide dynamic range, and remote access. Moreover, because the light is composed of photons, it does not carry any electrical charge and is immune to electromagnetic fields [5]. Due to these properties, FOS offer a completely passive (dielectric) approach, which is often very important in successful applications, including electrical isolation of patients in medicine, elimination of conductive paths in high-voltage environments and simple ways to adapt to existing materials. In addition, they are suitable for multi-point detection with their ability to easily connect to sensor arrays.

New optical fiber sensor technologies are also developed in the

literature using different materials. One of these is a study that provides a dynamic mechanical analysis of polymer optical fibers to obtain Young's modulus in terms of voltage, temperature, humidity, and frequency variation [6]. The multimode sensor for relative humidity is fabricated by fusion splicing a coreless fiber section to a single mode fiber [7]. Most of the FOS in dynamic pressure measurement are based on the principle of Fabry-Perot (FP) interferometry [8,9]. In addition, there are many current studies based on fiber Bragg grating technology [10–13]. Many diaphragm-based studies with different geometric sizes and materials are available in the literature [14,15]. Some of the studies with these diaphragm-based sensors are gas detection [16], underwater applications [17], partial discharge in power transformers [18] and they have spread over a wide area based on their measurements.

Many applications based on sound source localization (SSL) have been the focus of researchers for a long time. Among them, there are researches about robotic applications [19,20], teleconferencing, search and rescue activities, gunshot detection [21] and partial discharge [22]. Also, one crucial step for non-destructive testing technique and structural health monitoring is acoustic source localization in an anisotropic plate without knowing its material properties [23]. Thanks to the advantages of the FOS, they are also used in SSL applications [24]. In addition to the sensor equipment that forms the hardware structure of SSL, there is also a software part based on the processing of the signals obtained from this equipment. The main methods used for SSL are cross-correlation [25], genetic algorithm (GA) [26], maximum-

* Corresponding author.

E-mail addresses: sehayber@ahievran.edu.tr, skeser@ahievran.edu.tr (S.E. Hayber).

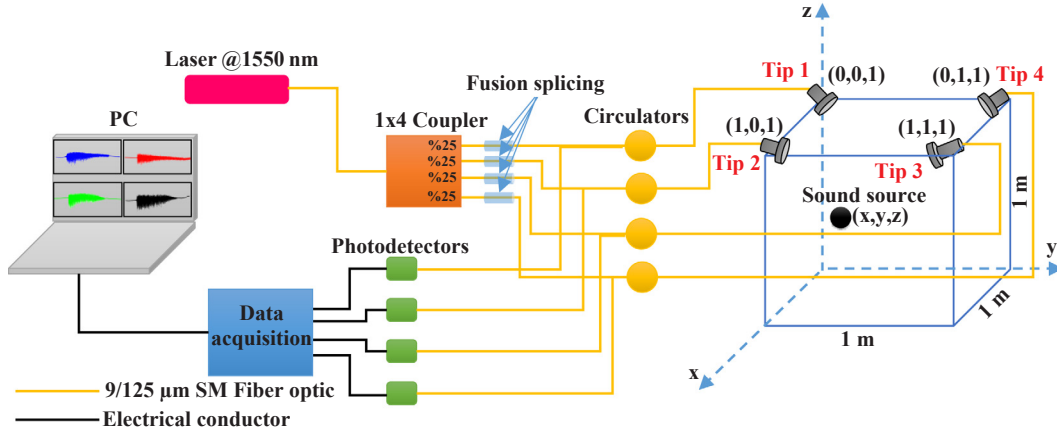


Fig. 3. The schematic diagram of the experimental setup with the FOS array system for SSL.

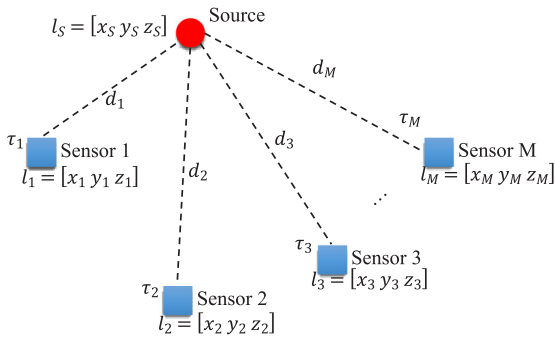


Fig. 4. Time delays based on sensor and source coordinates.

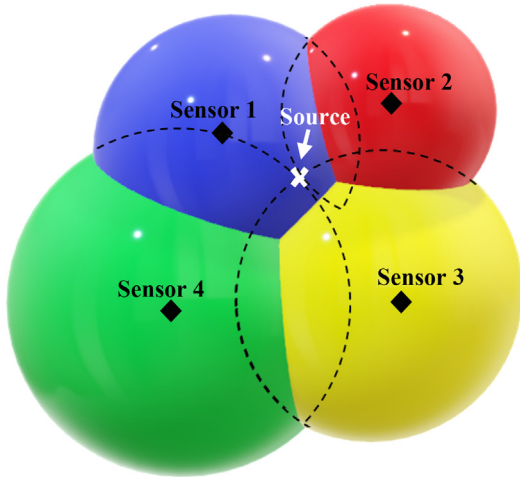


Fig. 5. The intersection of four imaginary spheres.

values between the sensors can be written as follows:

$$\tau_{ri} = \tau_i - \tau_r = \frac{d_i - d_r}{v} \quad (2)$$

τ_i and τ_r are the arrival time of the sound signal from the source to the i -th sensor and reference sensor, respectively. d_i and d_r are the distances of the i -th and reference sensors to the source, respectively. v is the sound velocity in the air, which is 343 m/s. i -th sensor distance (d_i) can be calculated as,

$$d_i = d_r + \tau_{ri} \times v \quad (3)$$

when both sides are squared,

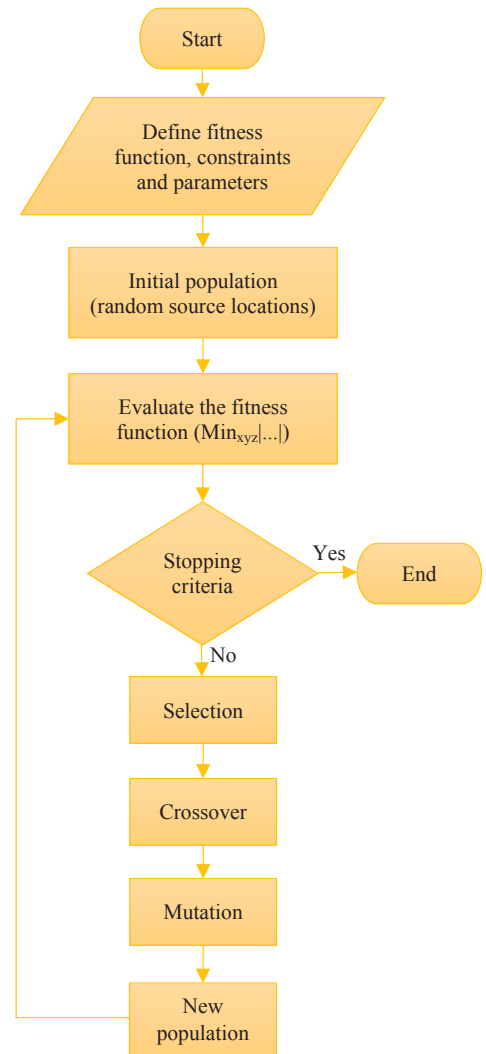


Fig. 6. Flow chart of genetic algorithm.

$$(d_i)^2 = (x_i - x_s)^2 + (y_i - y_s)^2 + (z_i - z_s)^2 = (d_r + \tau_{ri} \times v)^2, \quad i = 1, 2, \dots, M \quad (4)$$

is obtained. As a result of the necessary mathematical operations, Eq. (4) can be converted into the following matrix form (Eq. (5)).

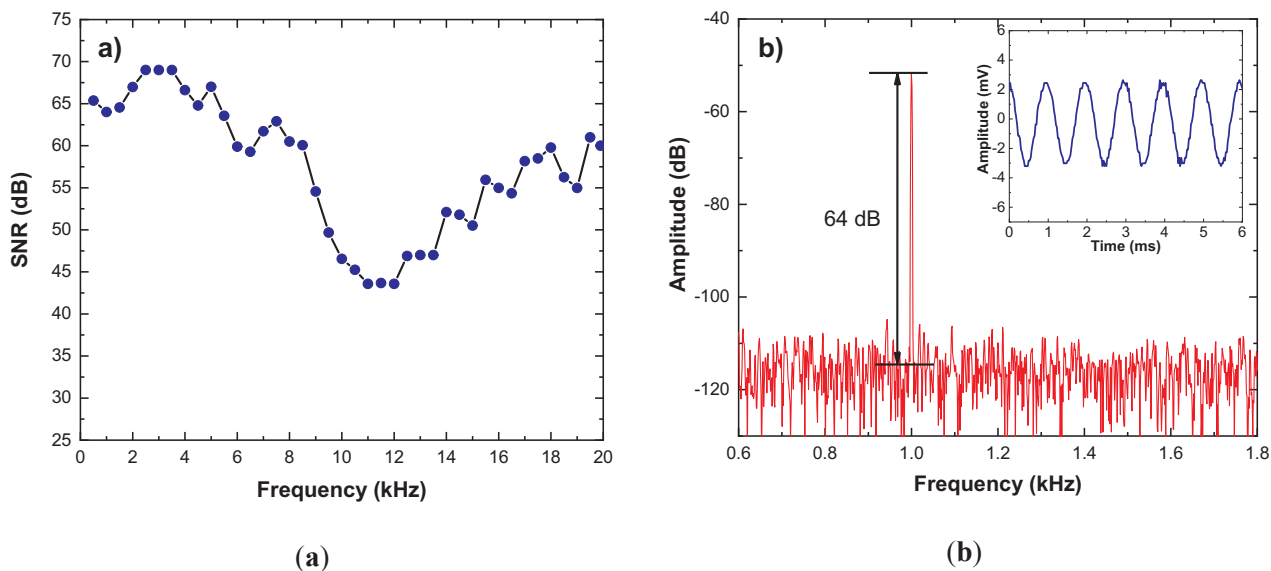


Fig. 7. Frequency response of the FOS: (a) from 100 Hz to 20 kHz; (b) at 1 kHz.

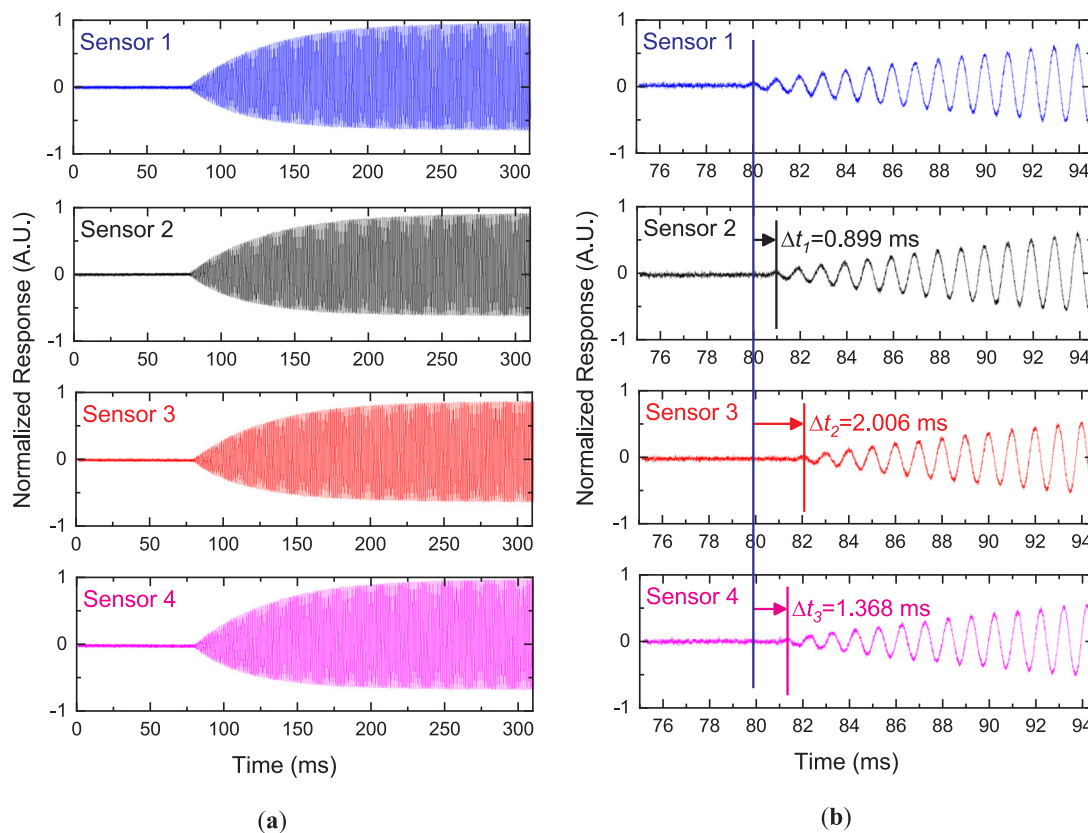


Fig. 8. The time-domain responses of four FOSs when the 1 kHz sound source signal appears at the setting position of Source 1 (0.2 m, 0 m, 0.2 m): (a) time scale from 0 to 310 ms; (b) time scale from 75 to 94.5 ms.

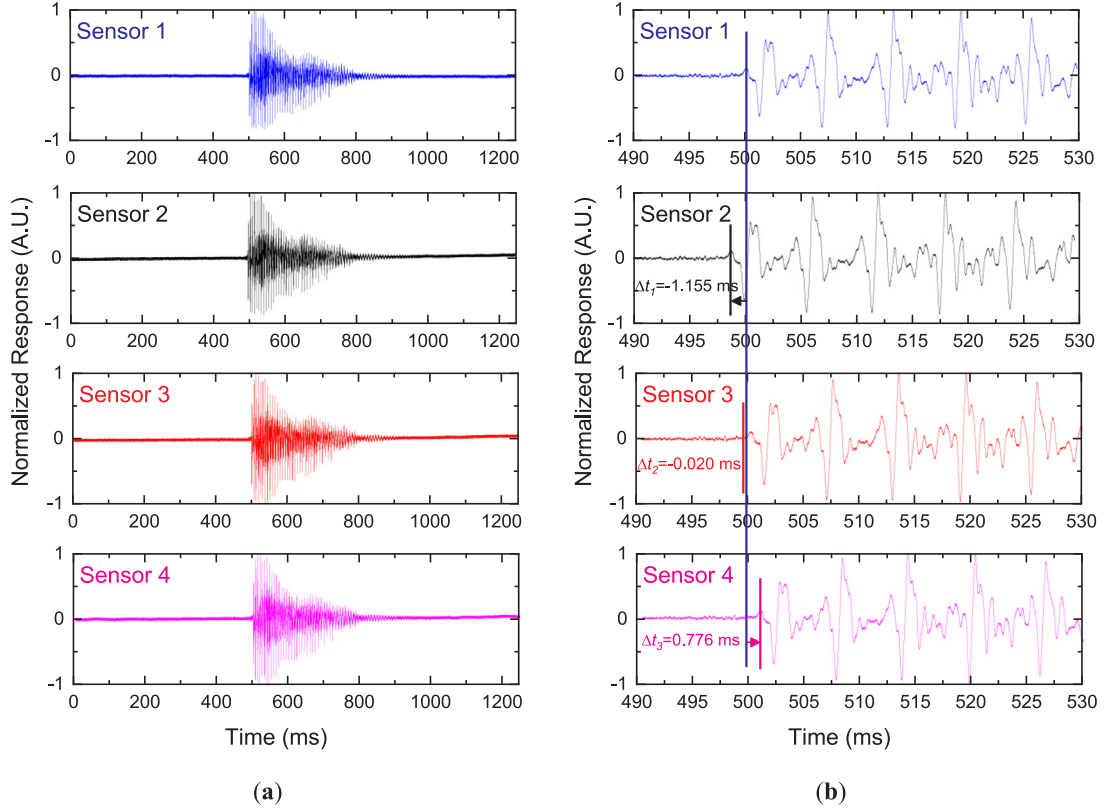


Fig. 9. The time-domain responses of four FOS when the bi (bi) speech signal appears at the setting position of Source 4 (0.8 m, 0.2 m, 0.5 m): (a) time scale from 0 to 1250 ms; (b) time scale from 490 to 530 ms.

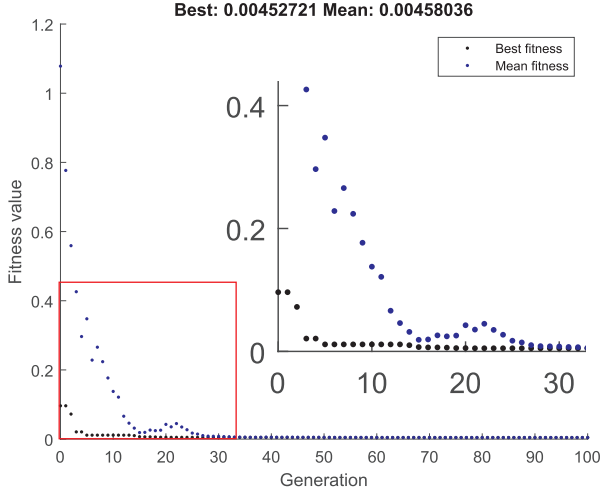


Fig. 10. Fitness values converging iteratively to zero.

$$\begin{aligned}
 & \text{Best: } 0.00452721 \text{ Mean: } 0.00458036 \\
 & \begin{matrix} \bullet & \text{Best fitness} \\ \bullet & \text{Mean fitness} \end{matrix} \\
 & \begin{matrix} 1.2 \\ 1.0 \\ 0.8 \\ 0.6 \\ 0.4 \\ 0.2 \\ 0 \end{matrix} \\
 & \begin{matrix} 0 & 10 & 20 & 30 & 40 & 50 & 60 & 70 & 80 & 90 & 100 \end{matrix} \\
 & \text{Generation}
 \end{aligned}$$

$$\begin{aligned}
 & \begin{bmatrix} 2(x_2 - x_r) & 2(y_2 - y_r) & 2(z_2 - z_r) & -2v\tau_{r2} \\ 2(x_3 - x_r) & 2(y_3 - y_r) & 2(z_3 - z_r) & -2v\tau_{r3} \\ \vdots & \vdots & \vdots & \vdots \\ 2(x_M - x_r) & 2(y_M - y_r) & 2(z_M - z_r) & -2v\tau_{rM} \end{bmatrix} \begin{bmatrix} x_s \\ y_s \\ z_s \\ d_r \end{bmatrix} \\
 & = \begin{bmatrix} x_2^2 + y_2^2 + z_2^2 - x_r^2 - y_r^2 - z_r^2 - v^2\tau_{r2}^2 \\ x_3^2 + y_3^2 + z_3^2 - x_r^2 - y_r^2 - z_r^2 - v^2\tau_{r3}^2 \\ \vdots \\ x_M^2 + y_M^2 + z_M^2 - x_r^2 - y_r^2 - z_r^2 - v^2\tau_{rM}^2 \end{bmatrix} \quad (5)
 \end{aligned}$$

Eq. (5) can be solved by the least squares method. The least squares

method provides the algebraic solution for SSL using TDOA measurements and can be written in the following matrix form

$$\mathbf{A}^T \mathbf{A} \mathbf{x} = \mathbf{A}^T \mathbf{b} \quad (6)$$

and,

$$\hat{\mathbf{x}} = (\mathbf{A}^T \mathbf{A})^{-1} \mathbf{A}^T \mathbf{b} \quad (7)$$

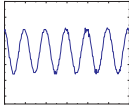
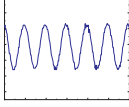
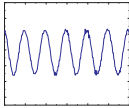
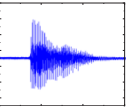
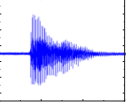
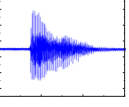
Since Eq. (5) contains four unknowns (x_s, y_s, z_s, d_r), M must be higher than or equal to four ($M \geq 4$) to find a solution. That is, at least 3 sensors and 4 sensors are required for 2D and 3D detection, respectively [36]. As can be seen in Fig. 5, three spherical shapes (Sensor 1, 2, and 3) intersect at two points. These two points represent possible source coordinates. One of these two possible points corresponds to the source position. As a result, this source position is determined using a fourth sensor (Sensor 4).

When the number of sensors is increased (M), the position of the source can be found with less error. However, this situation increases the computational complexity and computation time. With the least squares method, the global solution cannot always be reached correctly. Therefore, various optimization methods such as GA or particle swarm optimization, which give better results in terms of reaching the global solution, are preferred more.

2.3. Genetic algorithm (GA)

Genetic algorithm (GA) is a searching and optimization method that works in a similar way to the evolutionary process observed in nature [26]. The GA usually starts from a population of randomly generated individuals, and is an iterative process, with the population in each iteration called a generation [30]. GA has a fitness function that contains the solution space. In each generation, the fitness of each individual in the population is evaluated, and this fitness value is the value of the optimization function (fitness function). Then the new

Table 1
Sound source location results.

		Location results (m)					Distance results (m)					Average distances
		Experiment No.					Experiment No.					
	Source 1 (Fig. 8)	1	2	3	4	5	1	2	3	4	5	Source 1
x(m)	0.2	0.204	0.21	0.216	0.215	0.201	0.0166	0.0424	0.0402	0.0279	0.0046	0.0264
y(m)	0	0.006	0.016	0.024	0.023	0.002						
z(m)	0.2	0.215	0.238	0.228	0.205	0.204						
												
	Source 2	1	2	3	4	5	1	2	3	4	5	Source 2
x(m)	0.6	0.599	0.599	0.598	0.599	0.598	0.0142	0.0473	0.0503	0.0292	0.0316	0.0345
y(m)	0	0.002	0.005	0.005	0.003	0.006						
z(m)	0.9	0.914	0.947	0.95	0.929	0.931						
												
	Source 3	1	2	3	4	5	1	2	3	4	5	Source 3
x(m)	0.3	0.303	0.301	0.3	0.303	0.302	0.0168	0.0071	0.0032	0.0228	0.0166	0.0133
y(m)	0.8	0.796	0.799	0.799	0.795	0.796						
z(m)	0.1	0.116	0.107	0.103	0.122	0.116						
												
	Source 4 (Fig. 9)	1	2	3	4	5	1	2	3	4	5	Source 4
x(m)	0.8	0.814	0.808	0.792	0.788	0.814	0.0247	0.0330	0.0321	0.0481	0.0164	0.0309
y(m)	0.2	0.186	0.192	0.208	0.212	0.186						
z(m)	0.5	0.45	0.469	0.53	0.545	0.449						
												
	Source 5	1	2	3	4	5	1	2	3	4	5	Source 5
x(m)	0.7	0.703	0.691	0.705	0.705	0.698	0.0192	0.0514	0.0301	0.0203	0.0128	0.0268
y(m)	0.1	0.094	0.116	0.09	0.119	0.104						
z(m)	0.4	0.382	0.448	0.372	0.405	0.412						
												
	Source 6	1	2	3	4	5	1	2	3	4	5	Source 6
x(m)	0.8	0.81	0.805	0.789	0.791	0.794	0.0191	0.0153	0.0249	0.0122	0.0149	0.0173
y(m)	0.9	0.888	0.912	0.92	0.908	0.896						
z(m)	0.6	0.589	0.608	0.61	0.598	0.613						
												

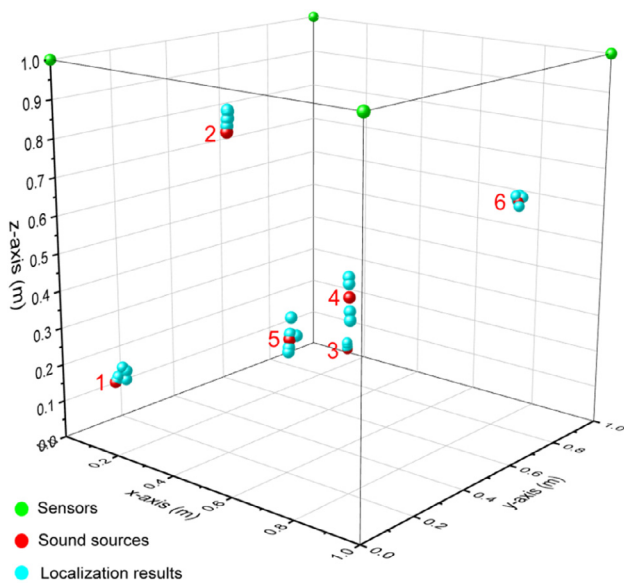


Fig. 11. 3D sound source location results.

generation of candidate solutions is used in the next iteration of the algorithm. The algorithm ends when a maximum number of generations are generated or when a valid fitness value for the population is reached.

Generally, measurement errors and sensor location errors occur in SSL applications. Therefore, a strong optimization method such as GA, which can research many solution points, is needed. This optimization process was carried out using the fitness function given below.

$$\min_{x, y, z} \sqrt{(x_i - x_s)^2 + (y_i - y_s)^2 + (z_i - z_s)^2} - v\tau_{ri} - d_r \quad (8)$$

$$i = 1, 2, \dots, M$$

where M is the number of sensors, (x_s, y_s, z_s) is the coordinate of the sound source, (x_i, y_i, z_i) is the coordinate of the i -th sensor. In Eq. (8), the genetic algorithm finds the optimal position that gives the minimum value of the fitness function. The flow chart of the genetic algorithm applied in experimental studies is given in Fig. 6. First of all, the fitness function, constraints, and necessary parameters for the GA are determined. Then, an initial population (a candidate solution set) is created. This set generates random source locations for constraints used in the study. The fitness function value is calculated for each chromosome and the chromosome that gives the most suitable fitness value is selected. This chromosome corresponds to the candidate source position. This chromosome value is retained as a local solution, thereby testing the stop criterion. In the algorithm, the process is terminated when a value smaller than the fitness value is reached or when the desired number of generations is reached. The local solution found is assigned as a global solution and if the criteria is not fulfilled, the next step is taken to continue looking for new solutions. In the population, the roulette wheel method is used for crossover. The selected individuals are subjected to crossover and mutation operators to create new

individuals and Step 2 is taken. Finally, the algorithm ends and the chromosome value that gives the best fitness value is selected. This value corresponds to the source position in this study.

3. Experimental results and discussion

3.1. Frequency response of the FOS array

The four sensor tips are manufactured through identical fabrication processes using diaphragm materials of the same standards. In the single FOS system of Fig. 2, sound signals are applied to Sensor 1 in the range of 100 Hz–20 kHz and the frequency response in Fig. 7(a) is obtained. This process is repeated for other sensors (Sensor 2, Sensor 3, and Sensor 4), and it is observed that the SNR values of each sensor are very close to the values obtained for Sensor 1. Therefore, it is understood from these results that the sensors have similar sensitivity. In addition, the sensors are located 10 cm away from the source that produces a constant frequency sound signal. Then, time delays are measured for each sensor and values very close to the speed of sound are obtained. As a result of this process, the calibration of the sensors is ensured. After these operations, we use the 1 kHz frequency signal, which has one of the higher SNR values, in the SSL system in Fig. 3. Frequency and time domain representation of the signal is given in Fig. 7(b).

3.2. Sound source localization (SSL)

The sound source of 1 kHz is placed in the coordinate Source 1 ($x = 0.2$ m, $y = 0$ m, $z = 0.2$ m), and the signal obtained simultaneously from the FOS tips is shown in Fig. 8(a). In Fig. 8(b), the time difference (TDOA) values are given according to the reference sensor (Sensor 1) selected. Also, a total of 15 measurements were performed by changing the source position to Source 2 ($x = 0.6$ m, $y = 0$ m, $z = 0.9$ m) and Source 3 ($x = 0.3$ m, $y = 0.8$ m, $z = 0.1$ m) to be 5 measurements for each location.

In our experimental study, in addition to the constant frequency sound signal, we also used a variable frequency speech signal (bi) to test the FOS array dynamic field performance. The sound source of the speech signal is placed in the coordinate Source 4 ($x = 0.8$ m, $y = 0.2$ m, $z = 0.5$ m), and the signal obtained simultaneously from the FOS tips is shown in Fig. 9(a). In Fig. 9(b), the time difference (TDOA) values are given based on the reference sensor (Sensor 1) selected. Besides, the measurements were repeated by changing the source position as Source 5 ($x = 0.7$ m, $y = 0.1$ m, $z = 0.4$ m) and Source 6 ($x = 0.8$ m, $y = 0.9$ m, $z = 0.6$ m). Similarly, multiple measurements were implemented for each location.

The fitness function Eq. (8) is minimized by using TDOA data obtained as a result of multiple measurements as well as sensor coordinates information. In the processes, the sound velocity value was taken as $v = 343$ m/s and the test operations were carried out at room temperature suitable for the sound velocity MATLAB's GA tool (genetic algorithm optimization toolbox (GAOT)) was used in calculations. The number of population (chromosome) is chosen as 100, the crossover constant is 0.85 and the number of generation (= number of iteration) is 100. Roulette wheel method was used to determine individuals to be crossed for the next generation to be created. In Fig. 10, when calculating Source 1 position, fitness value is converted iteratively to zero. Fig. 10 shows that the mean fitness value stably converges to zero after the 26th iteration.

A summary of the experimental studies can be found in Table 1. Measurement results for Source 1 and Source 4 are detailed in Figs. 8 and 9, respectively. Table 1 gives location results, distance results, and average distances. When 30 measurements were evaluated, it was found that 50 percent of the measurements remained below 0.02 m. In only two of these measurements, distances to the source were measured around 0.05 m and the average of all measurements was calculated as

0.0248 m. Also, the average distance to the source points was 0.0345 m, with the maximum error, while the minimum was 0.0133 m. The causes of errors can include sensor sensitivity, different sensor and source positions from actual positions, and small measurement errors in synchronization. As the distance between the sensors decreases, the TDOA values will be very close to each other and the error rate in the measurements will increase. For this reason, sensor positions have been chosen as far distance as possible.

Fig. 11 shows the measurement results for variable source points in 3D space, here, the green, red, and cyan points show the sensor, sound source, and localization results, respectively. Measurements were repeated 5 times for each source position and a total of 30 measurements were performed for 6 source positions. In the first three of these source positions, a constant frequency (1 kHz) signal was used, and in others, a speech (bi) signal was used.

4. Conclusion

In this study, sensing tips were performed by using EPDM, a material that is easy to manufacture and resistant to heavy working conditions. A 4-element sensor array was obtained from these sensor tips. The signal acquisition and processing unit is designed simply and cost-effectively. A test box with a size of 1 m³ was chosen as the measurement area. The location of the sound source placed in the test box was changed to 3D and multiple SSL measurements were implemented for each of these locations. In the study, both constant frequency and a speech signal were used. The signals obtained from the sensor array are processed with a genetic algorithm that scans the global solution space multiple and can find the global solution effectively. The largest of the average distances to the source points was 0.0345 m, while the smallest was 0.0133 m. In addition, the distance to the source point in 14 of 30 measurements remained below about 0.02 m. Our next study will be carried out to determine the source position using the 5th sensor in the cases where TDOA values are very close to each other, that is when the distance of the sensors is equal to the source.

Declaration of Competing Interest

The authors declare that they have no known competing financial interests or personal relationships that could have appeared to influence the work reported in this paper.

Acknowledgments

This work was supported by the Research Fund of the Kırşehir Ahi Evran University, Turkey. Project numbers KMY.A4.19.001. The authors would like to thank FOSENS Electro Optic Technologies for their supports in the research activities among the staff.

References

- [1] H. Kuttruff, *Acoustics: An Introduction*. CRC Press, 2006, 457 pp.
- [2] G. Wild, S. Hinckley, Acousto-ultrasonic optical fiber sensors: overview and state-of-the-art, *IEEE Sens. J.* 8 (7) (2008) 1184–1193.
- [3] J.G. Teixeira, et al., Advanced fiber-optic acoustic sensors, *Photon. Sens.* 4 (3) (2014) 198–208.
- [4] J. Fraden, *Handbook of Modern Sensors: Physics, Designs, and Applications*, Springer Science & Business Media, 2004, p. 663.
- [5] E. Udd, W.B. Spillman Jr., *Fiber Optic Sensors: An Introduction for Engineers and Scientists*, John Wiley & Sons, 2011, p. 498.
- [6] A. Leal-Junior, A. Frizera, M.J. Pontes, A. Fasano, G. Woyessa, O. Bang, C.A.F. Marques, Dynamic mechanical characterization with respect to temperature, humidity, frequency and strain in mPOFs made of different materials, *Opt. Mater. Express* 8 (4) (2018) 804–815.
- [7] S. Novais, M.S. Ferreira, J.L. Pinto, Relative humidity fiber sensor based on multimode interferometer coated with agarose-gel, *Coatings* 8 (12) (2018) 453.
- [8] C.A. Díaz, C. Leitão, C.A. Marques, M.F. Domingues, N. Alberto, M.J. Pontes, P.F. Antunes, Low-cost interrogation technique for dynamic measurements with FBG-based devices, *Sensors* 17 (10) (2017) 2414.
- [9] M.F. Domingues, C.A. Rodriguez, J. Martins, C. Tavares, C. Marques, N. Alberto,

- P. Antunes, Cost-effective optical fiber pressure sensor based on intrinsic Fabry-Perot interferometric micro-cavities, *Opt. Fiber Technol.* 42 (2018) 56–62.
- [10] C.A.F. Marques, R. Min, A.L. Junior, P. Antunes, A. Fasano, G. Woyessa, O. Bang, Fast and stable gratings inscription in POFs made of different materials with pulsed 248 nm KrF laser, *Opt. Express* 26 (2) (2018) 2013–2022.
- [11] A. Leal-Junior, A. Theodosiou, A. Frizzera-Neto, M.J. Pontes, E. Shafir, O. Palchik, P. André, Characterization of a new polymer optical fiber with enhanced sensing capabilities using a Bragg grating, *Opt. Lett.* 43 (19) (2018) 4799–4802.
- [12] A. Leal-Junior, A. Theodosiou, C. Dfaz, C. Marques, M.J. Pontes, K. Kalli, A. Frizzera-Neto, Polymer optical fiber Bragg gratings in CYTOP fibers for angle measurement with dynamic compensation, *Polymers* 10 (6) (2018) 674.
- [13] A.G. Leal-Junior, A. Theodosiou, C. Marques, M.J. Pontes, K. Kalli, A. Frizzera, Compensation method for temperature cross-sensitivity in transverse force applications with FBG sensors in POFs, *J. Lightwave Technol.* 36 (17) (2018) 3660–3665.
- [14] Q. Wang, Q. Yu, Polymer diaphragm based sensitive fiber optic Fabry-Perot acoustic sensor, *Chin. Opt. Lett.* 8 (3) (2010) 266–269.
- [15] K.K. Chin, et al., Fabry-Perot diaphragm fiber-optic sensor, *Appl. Opt.* 46 (31) (2007) 7614–7619.
- [16] Z. Gong, et al., Photoacoustic spectroscopy based multi-gas detection using high-sensitivity fiber-optic low-frequency acoustic sensor, *Sens. Actuators B* 260 (1) (2018) 357–363.
- [17] F. Wang, et al., Extrinsic Fabry-Pérot underwater acoustic sensor based on micro-machined center-embossed diaphragm, *J. Lightwave Technol.* 32 (23) (2014) 4026–4034.
- [18] J. Deng, et al., Optical fiber sensor-based detection of partial discharges in power transformers, *Opt. Laser Technol.* 33 (5) (2001) 305–311.
- [19] C.C. Liu, J.R. Cheng, J.F. Huang, Integrating correlation acquisition with location optimization for accurate indoor lightwave robot positioning, *Proc. Comput. Sci.* 110 (2017) 304–311.
- [20] G. Chen, Y. Xu, A sound source localization device based on rectangular pyramid structure for mobile robot, *J. Sens.* (2019).
- [21] G. Valenzise, et al., Scream and gunshot detection and localization for audio-surveillance systems, in: 2007 IEEE Conference on Advanced Video and Signal Based Surveillance 21–26.
- [22] L. Song, et al., Position location of partial discharges in power transformers using fiber acoustic sensor arrays, *Opt. Eng.* 45 (11) (2006) 114401.
- [23] W.H. Park, P. Packo, T. Kundu, Acoustic source localization in an anisotropic plate without knowing its material properties – a new approach, *Ultrasonics* 79 (2017) 9–17.
- [24] J. Wang, et al., Sound source localization based on Michelson fiber optic interferometer array, *Opt. Fiber Technol.* 51 (2019) 112–117.
- [25] Y.T. Chang, C.L. Wu, H.C. Cheng, The enhanced locating performance of an integrated cross-correlation and genetic algorithm for radio monitoring systems, *Sensors* 14 (4) (2014) 7541–7562.
- [26] L. Davis, *Handbook of Genetic Algorithms*, Van Nostrand Reinhold, New York, USA, 1991.
- [27] H. Cao, Y.T. Chan, H.C. So, Maximum likelihood TDOA estimation from compressed sensing samples without reconstruction, *IEEE Signal Process. Lett.* 24 (2017) 564–568.
- [28] O.A. Oumar, M.F. Siyau, T.P. Sattar, Comparison between MUSIC and ESPRIT direction of arrival estimation algorithms for wireless communication systems, in: *The First International Conference on Future Generation Communication Technologies*, IEEE, 2012, pp. 99–103.
- [29] D.E. Goldberg, *Genetic Algorithms in Search, Optimization, and Machine Learning*, Addison-Wesley, USA, 1989, pp. 1–25.
- [30] M.D. Vose, *The Simple Genetic Algorithm, Foundations and Theory*. MIT Press, Cambridge, MA, 1999.
- [31] S.E. Hayber, T.E. Tabaru, O.G. Saracoglu, A novel approach based on simulation of tunable MEMS diaphragm for extrinsic Fabry-Perot sensors, *Opt. Commun.* 430 (2019) 14–23.
- [32] S.E. Hayber, et al., The experimental validation of designed fiber optic pressure sensors with EPDM diaphragm, *IEEE Sens. J.* 19 (14) (2019) 5680–5685.
- [33] J.-R.R. Ruiz, T. Canals, R. Cantero, Supervision of ethylene propylene diene M-class (EPDM) rubber vulcanization and recovery processes using attenuated total reflection Fourier transform infrared (ATR FT-IR) spectroscopy and multivariate analysis, *Appl. Spectrosc.* 71 (1) (2017) 141–151.
- [34] M. Rosić, M. Simić, P. Pejović, Hybrid genetic optimization algorithm for target localization using TDOA measurements, *Proceedings of the IcETRAN*, (2017).
- [35] N. Patwari, et al., Locating the nodes: cooperative localization in wireless sensor networks, *Signal Process. Mag. IEEE* 22 (4) (2005) 54–69.
- [36] P. Strumillo, *Advances in Sound Localization*, InTech, 2011.